

Journal of Geophysical Research: Space Physics

RESEARCH ARTICLE

10.1002/2017JA024284

Key Points:

- Rocket's floating potential decreases in the presence of a magnetic field perpendicular to plasma flow direction
- The wake in potential and density may extend as far as 30 Debye lengths, which can influence the in situ measurements
- The wake in the presence of magnetic field is asymmetric downstream of the rocket

Correspondence to:D. Darian,
diakod@math.uio.no**Citation:**

Darian, D., S. Marholm, J. J. P. Paulsson, Y. Miyake, H. Usui, M. Mortensen, and W. J. Miloch (2017), Numerical simulations of a sounding rocket in ionospheric plasma: Effects of magnetic field on the wake formation and rocket potential, *J. Geophys. Res. Space Physics*, 122, 9603–9621, doi:10.1002/2017JA024284.

Received 21 APR 2017

Accepted 14 AUG 2017

Accepted article online 17 AUG 2017

Published online 8 SEP 2017

Numerical simulations of a sounding rocket in ionospheric plasma: Effects of magnetic field on the wake formation and rocket potential

D. Darian¹ , S. Marholm² , J. J. P. Paulsson², Y. Miyake³ , H. Usui³ , M. Mortensen¹, and W. J. Miloch²

¹Department of Mathematics, University of Oslo, Oslo, Norway, ²Department of Physics, University of Oslo, Oslo, Norway,

³Department of Computational Science, Kobe University, Kobe, Japan

Abstract The charging of a sounding rocket in subsonic and supersonic plasma flows with external magnetic field is studied with numerical *particle-in-cell* (PIC) simulations. A weakly magnetized plasma regime is considered that corresponds to the ionospheric F_2 layer, with electrons being strongly magnetized, while the magnetization of ions is weak. It is demonstrated that the magnetic field orientation influences the floating potential of the rocket and that with increasing angle between the rocket axis and the magnetic field direction the rocket potential becomes less negative. External magnetic field gives rise to asymmetric wake downstream of the rocket. The simulated wake in the potential and density may extend as far as 30 electron Debye lengths; thus, it is important to account for these plasma perturbations when analyzing in situ measurements. A qualitative agreement between simulation results and the actual measurements with a sounding rocket is also shown.

1. Introduction

With in situ measurements it is possible to directly study dynamic plasma phenomena in the ionosphere. Such studies are of interest for both space weather applications [Hey *et al.*, 1946; Kintner *et al.*, 2007; Prikryl *et al.*, 2011] and general understanding of plasma waves and turbulence [de Leeuw, 1967; Stone, 1981; Chen, 1965; Chung *et al.*, 1974]. Due to accessibility, lower parts of the Earth's ionosphere can be studied in situ only with sounding rockets. Over several decades, many sounding rocket experiments have been performed which allowed for in situ measurements of plasma density, temperature, drift velocities, or electromagnetic fields and improved our understanding of many processes in the ionosphere [Oya, 1970; Svenes *et al.*, 1990; Yamamoto, 2001; Endo *et al.*, 2015; Moen *et al.*, 2012; Spicher *et al.*, 2015; Lorentzen *et al.*, 2010; Oksavik *et al.*, 2012].

A sounding rocket, just as any other finite-sized object, will interact with the surrounding plasma [Gurevich *et al.*, 1969; Hastings, 1995]. This may lead to disturbances in the vicinity of the rocket, and examples of those are wake formation and sheath effects [Al'pert *et al.*, 1963; Liu, 1969]. In situ measurements of ionospheric plasma density and temperature by Langmuir probes installed on sounding rockets or satellites are, in certain situations, perturbed by the presence of the rapidly moving rocket or satellite itself [Svenes *et al.*, 1990; Svenes and Trøim, 1994; Endo *et al.*, 2015]. However, because of the complexity of the problem of the plasma-object interaction, most of the theoretical analysis is limited to simplified and idealized conditions [Hastings, 1995]. In addition to the perturbations caused by the rocket or satellite itself, there are perturbations due to the wake formation of the probes [Meyer-Vernet, 1976]. Finally, the presence of a background magnetic field \mathbf{B}_0 , and the corresponding convective electric field $\mathbf{E}_0 = -\mathbf{v}_D \times \mathbf{B}_0$ (\mathbf{v}_D being the drift velocity) can significantly influence the plasma-particle dynamics [Miller, 1971; Whipple, 1965; Lafon, 1973]. These complex interactions can affect in situ experiments in the ionosphere; it is therefore crucial in analyzing results from such experiments, to have a proper understanding of plasma-rocket interactions and related phenomena [Al'pert *et al.*, 1963; Temerin and Kintner, 1989; Hasegawa, 1975; Meyer-Vernet, 1976].

The interaction between plasmas and solid objects, such as rockets, satellites, probes, moons, asteroids, or dust grains, remains one of the main problems in plasma and space physics [Garrett, 1981; Whipple, 1981], and while in the present study we focus on the plasma-object interaction, our results can be generalized to account

for other finite-sized objects. One of the outstanding problems in studying plasma-object interactions, is the role of the magnetic field on the charging process and the wake formation. In particular, the plasma-rocket interaction under such conditions becomes nontrivial. Thus, in this paper we employ self-consistent, numerical, particle-in-cell (PIC) simulations to address this problem. We study the potential on the rocket and wake formation in subsonic and supersonic plasma flows corresponding to a rocket moving through the F_2 layer of the ionosphere.

1.1. Charging of the Rocket Surface

A sounding rocket in the ionosphere will in general be negatively charged because of the electrons' large mobility as compared to ions. Under usual ionospheric conditions, the ions and electrons from the ambient plasma that are incident on the rocket surface, electrons emitted by photoemission and secondary emission, and backscattered electrons, will determine the charge of the rocket. The current balance equation, which defines surface charging, is given by [Escoubet *et al.*, 1997]

$$I_T(\Phi_S) = I_e(\Phi_S) - (I_i(\Phi_S) + I_{ph}(\Phi_S) + I_{se}(\Phi_S) + I_{bse}(\Phi_S)), \quad (1)$$

where Φ_S is the surface potential relative to ambient plasma potential, I_T is the total current to rocket surface, I_e and I_i are the incident electron and ion currents, respectively, I_{ph} is the current of photoelectrons, I_{se} is the current of secondary electrons, and I_{bse} is the current of backscattered electrons. We are primarily interested in the lower ionospheric regions, where the ambient electron current density is of the order of milliamperes per square meter [Hastings, 1995; Anderson, 2012], whereas the electron current density due to photoemission for various spacecraft/rocket materials is of the order of microamperes per square meter [Grard, 1973]. Furthermore, the photoemission is proportional to the photon flux, while electron/ion currents are functions of the background plasma density, which is relatively high in the F layer [Hastings, 1995]. The current density from secondary and backscattered electrons produced by energetic electrons incident on the rocket surface is also usually insignificant compared to the ambient electron and ion currents [Hastings, 1995; Anderson, 2012]. Therefore, for lower ionospheric plasma conditions the currents from ambient plasma particles (i.e., electrons and ions) generally dominate, and one can often neglect contributions from the photoemission and other currents.

At equilibrium, when the net current to the surface is negligible, i.e., $I_T \approx 0$, the potential on the surface reaches the so-called *floating potential* [Whipple, 1981]. For the charging conditions described above, the floating potential on a rocket will be negative, and the resulting electric field close to the surface will repel the surplus of electrons and accelerate ions toward the surface. Consequently, the region closest to the surface is characterized by an excess of positive charge that shields the negative charge accumulated on the rocket. This region of plasma around the rocket which has an increased density of ions is referred to as the *electrostatic sheath*. In stationary plasmas, the sheath of an isolated object extends to usually a few Debye lengths λ_D , where $\lambda_D = \sqrt{\epsilon_0 k_B T / ne^2}$, where k_B is the Boltzmann's constant, ϵ_0 is the electric constant, e is the elementary charge, n is the plasma density, and T is the plasma temperature. Thus, both the floating potential and the sheath thickness depend on the local plasma parameters.

In the ionosphere, the radius of the rocket is usually larger than the Debye length, $R \gg \lambda_D$, and the sheath is *thin* with respect to the size of the object. We will neglect collisions with the background, which is a sound assumption for the ionospheric F layer [Al'pert *et al.*, 1965]. In this limit, one can find the floating potential analytically, as will be shown in the following. All ions that enter the sheath will be neutralized on the surface. In order to fulfill the Bohm criterion, the ions reaching the sheath edge are accelerated to the critical velocity, which for cold ions is the *Bohm velocity*: $v_B = \sqrt{k_B T_e / m_i}$ [Riemann, 1991; Bohm *et al.*, 1949]. The symbols T_s , m_s , and n_s are used to denote temperature, mass, and density of species s (electron or ion), respectively. The ion current to a negatively charged (stationary) rocket is given by

$$I_i \simeq \alpha n_i e v_B A, \quad (2)$$

where A is the surface area of the rocket, and α is dependent on the temperature ratio T_e/T_i [Sugawara, 1998]. Energetic electrons can enter the sheath, and the electron current to the surface depends on the rocket's retarding potential

$$I_e \simeq -\frac{1}{4} n_e e \bar{v}_e A \exp\left(-\frac{e|\Phi - \Phi_{pl}|}{k_B T_e}\right), \quad (3)$$

where $\bar{v}_e = \sqrt{8k_B T_e / \pi m_e}$ is the mean velocity of the electrons, Φ is the electric potential in the sheath region, and Φ_{pl} is the undisturbed plasma potential far away and can be arbitrarily set to zero. When the electron current balances the ion current, the net current to the rocket becomes zero, and the rocket reaches floating potential Φ_{fl} , which is given by

$$\frac{e|\Phi_{fl} - \Phi_{pl}|}{k_B T_e} = -\frac{1}{2} \ln \left(2\pi\alpha^2 \frac{m_e}{m_i} \right). \quad (4)$$

Note that in the case where the radius of the rocket would be much smaller than the Debye length, $R \ll \lambda_D$, we need to consider the *thick sheath limit*, where the current is limited by particle orbits. That regime is called *orbit motion limited (OML)* [Mott-Smith and Langmuir, 1926; Bernstein and Rabinowitz, 1959; Bohm et al., 1949; Whipple, 1981; Allen et al., 2000]. However, the OML regime is not relevant for this study.

The first published calculations of the charging of a macroscopic object moving in a plasma was given by Lehnert [1956], who, by including the ion ram effects, estimated the spacecraft potential to be -0.7 to -1.0 V. Gringauz and Zelikman [1957] studied the electrostatic sheath and the distribution of charge around a spacecraft, and by taking into account the influence of the spacecraft velocity and photoemission derived an expression for the floating potential.

An accurate knowledge about the floating potential of spacecraft is crucial for plasma measurements, especially when the floating potential is comparable to the energy of the measured ambient plasma particles [Olsen et al., 1986; Cohen et al., 2016]. Equally important are the effects of the charged spacecraft, and its sheath, on the trajectories of plasma particles, which can be used to determine the plasma temperature [Comfort et al., 1982; Fernandes and Lynch, 2016]. Since the current equations presented above, equations (2) and (3), are only valid for stationary, i.e., nondrifting, unmagnetized and collisionless plasmas, we will, in the following, give more accurate expressions for the ion and electron currents in the case of a drifting and magnetized plasma, which then can be used to determine the floating potential of the spacecraft.

In the case of a drifting plasma, when the thermal velocity of ions is less than the drift velocity, the ions are primarily collected from the ram direction of the rocket, and the ion saturation current is approximately given by [Hoegy and Wharton, 1973; Brace, 1998]

$$I_i \simeq \frac{1}{4\sqrt{\pi}} n_i e \bar{v}_i A \left(\frac{1}{2} + \frac{m_i v_D^2}{2k_B T_i} + \frac{e(\Phi - \Phi_{pl})}{k_B T_i} \right)^{\frac{1}{2}}, \quad (5)$$

where v_D is the drift velocity. For a nondrifting collisionless plasma in the presence of a background magnetic field, an upper bound for the collected electron current to the rocket can be found [Parker and Murphy, 1967; Rubinstein and Laframboise, 1983], which is given by

$$I_e \simeq -\frac{1}{4} n e \bar{v}_e A \left(\frac{1}{2} + \frac{1}{2} \left(\frac{8e|\Phi - \Phi_{pl}|}{m_e \omega_{ce}^2 R^2} \right)^{\frac{1}{2}} + \frac{k_B T_e}{m_e \omega_{ce}^2 R^2} \right), \quad (6)$$

where R is the radius of the rocket and $\omega_{ce} = e|\mathbf{B}|/m_e$ is the electron gyrofrequency.

1.2. Wake Formation

A relative motion between the object and plasma will lead to wake formation in the downstream direction [Liu, 1969; Gurevich et al., 1969; Whipple, 1981]. The wake is due to absorption of charges on the object's surface and electrostatic interactions between the object and plasma particles, such as ion focusing effects [Miloch et al., 2008].

Wake formation behind finite-sized objects has been previously studied theoretically [e.g., Al'pert et al., 1963; Brundin, 1963; Al'pert et al., 1965; Liu, 1969; Grabowski and Fischer, 1974; Sanmartin, 1970; Szuszczewicz and Takacs, 1979; Rubinstein and Laframboise, 1983; Laframboise and Rubinstein, 1976; Tang and Delzanno, 2014] and experimentally in the ionosphere with satellites [Samir and Wrenn, 1972; Svenes et al., 1990] extending to very large space vehicles such as the Space Shuttle [Murphy et al., 1983; Siskind et al., 1984]. For a review on the plasma-spacecraft interactions at low Earth orbit the reader is referred to Hastings [1995] and Whipple [1981]. Note that there are also analytical works which are concerned with the linear response of plasma to point-like objects [Ishihara and Vladimirov, 1997; Guio et al., 2008; Vladimirov and Nambu, 1995; Lemons et al., 2000], which are relevant for the OML regime of thick sheath. Since the object charging is often nonlinear

and objects are of finite size, it is advantageous to study the problem with numerical simulations [Holmström *et al.*, 2012; Allen, 2012; Melandsø and Goree, 1995; Patacchini and Hutchinson, 2011; Guio *et al.*, 2008; Yaroshenko *et al.*, 2012; Miyake *et al.*, 2013]. For numerical studies of plasma-object interactions, it is usual to employ the particle-in-cell method, where the trajectories of a large number of plasma particles are computed in self-consistent electromagnetic or electrostatic fields [Birdsall and Langdon, 2004; Tajima, 1989; Jardin, 2010], thus allowing for first-principles studies. This approach is preferred for studies of spacecraft charging in flowing plasmas. However, so far most numerical studies have not considered any effects of an external magnetic field.

With two-dimensional numerical PIC simulations of spacecraft-plasma interaction in a dilute, weakly magnetized plasma, Okada *et al.* [1995] have shown that the electron to ion temperature ratio plays an important role in the formation of a wake. They considered the thick sheath limit, which is also relevant for the dust-charging experiments in laboratory experiments. In fact, a strong temperature ratio dependence of the wake has also been found for unmagnetized wakes forming behind dust grains [Maiorov *et al.*, 2000; Miloch, 2014, 2010; Melandsø and Goree, 1995]. In another study, Wang and Hastings [1992] used hybrid simulations to study the structure of the wake behind high-voltage space platforms in the ionosphere. Their simulations reveal that at high negative voltages, the wake is characterized by two ion-rich strips. Furthermore, the wake depends on the voltage, plate size, and angle relative to the flow, and ions in the wake can, under certain conditions, be focused back on the plate, which in turn may affect onboard instrumentation. Such effects of electrostatic lensing have also been observed for dusty plasmas, other spacecrafts, and instruments [Yaroshenko *et al.*, 2012; Miloch *et al.*, 2011; Block and Miloch, 2014].

To this day, wake formation in flowing magnetized plasmas has not been adequately addressed. For a spherical conducting object, Patacchini and Hutchinson [2011] have studied the ion collection in flowing magnetized plasmas, for the entire range of Debye length, using hybrid PIC simulations, where while the background electrons are treated as a fluid, the ions are considered to be Lagrangian particles. Marchand [2012] reported full PIC simulations of a spherical object in both stationary and drifting magnetized plasmas, with a constant external magnetic field, and demonstrated that the presence of the magnetic field results in a less negative floating potential.

One can expect that the magnetic field will have a significant effect for nonspherical objects. The effects of the magnetic field orientation on the object-plasma interactions still remain an open question [Al'pert *et al.*, 1965; Grabowski and Fischer, 1974]. It is of particular interest to understand how the orientation of magnetic field will affect the structure of the wake and the floating potential. An external magnetic field will restrict plasma dynamics, and magnetized electrons and/or ions will likely modify the currents to object's surface and the wake in flowing plasmas. Since the dynamics of ionospheric plasma is controlled to a large degree by the Earth's magnetic field, understanding this problem is of importance for in situ studies by sounding rockets and satellites. However, to the best of our knowledge, the effects of the orientation of the magnetic field on the wake formation and on the floating potential of a rocket have not been studied numerically before by three-dimensional first-principle particle simulations.

To address these problems we carry out three-dimensional full numerical PIC simulations of wake formation behind a cylindrically shaped rocket in the presence of an external magnetic field. We study the interaction between the rocket and drifting magnetized plasma by considering plasma parameters that can be related to the ionospheric *F* layer, and for different orientations of the rocket with respect to the magnetic field. We find that a magnetic field can introduce a noticeable asymmetry in the wake and can also influence the floating potential of the rocket. The simulated wake is extending far in the downstream direction, and thus can influence the in situ plasma measurements.

The remainder of the paper is organized as follows. The numerical method, simulation setup, and considered plasma parameters are introduced in section 2. In section 3, the results of the simulations are presented. A discussion of the results is given in section 4, followed by a summary and concluding remarks in section 5.

2. Numerical Setup

To study the problem of rocket-plasma interaction with numerical simulations, we use the electromagnetic spacecraft environment simulator (EMSES), which is a 3-D particle-in-cell (PIC) code [Miyake and Usui, 2009]. Particle-in-cell codes solve a characteristic of the Vlasov-Maxwell system of equations (i.e., collisionless

plasma) by initially sampling particle positions and velocities from the phase-space distribution and then numerically integrating the Lorentz force,

$$m_i \frac{d^2 \mathbf{x}_i}{dt^2} = q_i \left(\mathbf{E} + \frac{d\mathbf{x}_i}{dt} \times \mathbf{B} \right), \quad (7)$$

to get the trajectories $\{\mathbf{x}_i\}$ of all simulation particles. q_i and m_i are charge and mass of particle i , respectively. In EMSES, equation (7) is numerically integrated by the Boris-Buneman scheme [Boris, 1970] which is second-order accurate with respect to the numerical time step Δt .

In the general electromagnetic case, the magnetic field \mathbf{B} in equation (7) depends upon the position and velocities of the particles in the ensemble. In this study we are only concerned with electrostatic phenomena, and any magnetic field arising from the collective motion of the particles is neglected. However, we do take into account an external constant magnetic field \mathbf{B}_0 resembling that of the Earth.

The electric field \mathbf{E} , on the other hand, must be consistent with the particle distribution. The PIC method uses a four-step cycle when integrating the positions to achieve this: First, the charge of each particle is assigned to a grid to form a charge density ρ . In our case it is linearly distributed between the eight grid nodes surrounding it. Second, since we use the electrostatic approximation, Maxwell's equations reduce to the Poisson equation which is then solved numerically on this grid:

$$\nabla^2 \Phi = -\frac{\rho}{\epsilon_0}, \quad \mathbf{E} = -\nabla \Phi.$$

Third, the electric field is interpolated back onto the particles, again linearly from the eight nodes surrounding it, and finally, one can update the position one time step according to equation (7). The cycle must be repeated each time step. For further details about the PIC method we refer to *Birdsall and Langdon* [2004] and *Hockney and Eastwood* [1988].

At the center of the simulation box filled with magnetized plasma, we place a cylindrical body resembling a rocket, with a length of $42.5\lambda_D$ and a diameter of $15\lambda_D$, where λ_D denotes the Debye length of the background plasma. It is modeled as a perfect electric conductor, meaning that surface charges which it accumulates are instantaneously redistributed to maintain an equipotential over the body surface. This corresponds to an interior Dirichlet boundary where the boundary value is chosen according to charge conservation. However, to deal with the geometry of this boundary, EMSES uses the capacitance matrix method [Miyake and Usui, 2009].

Consider putting a unit point charge on surface node j , $\rho(\mathbf{x}) = \delta(\mathbf{x} - \mathbf{x}_j)$, and let $G_{ij} = G(\mathbf{x}_i, \mathbf{x}_j)$ be the resulting potential at surface node i (the Green's function), as determined analytically or, like in EMSES, by numerically solving for the unit point charge. Owing to the linearity of the Poisson equation or its discretized counterpart, the surface potential when several surface nodes has nonzero charge density ρ_j is

$$\Phi_i = \sum_j G_{ij} \rho_j. \quad (8)$$

When using the capacitance matrix method, the particles accumulated by the object is removed and their charge is put somewhere on the surface of the object. Solving the Poisson equation then yields a potential $\tilde{\Phi}$. In order to redistribute the surface charges, surface charge densities $\delta\rho_j$ are added to superimpose a potential $\delta\Phi_i = \Phi_c - \tilde{\Phi}_i$ on the surface, where Φ_c is the constant equipotential. $\delta\rho_j$ is found by solving equation (8). While Φ_c makes an additional unknown, requiring charge conservation, $\sum_j \delta\rho_j = 0$, closes the system of equations and makes the equipotential consistent. At last, the Poisson equation is solved again with the new charge density to obtain the correct potential Φ throughout the domain. For further details about the capacitance matrix we refer to *Hockney and Eastwood* [1988] and *Miyake and Usui* [2009].

While we simplify the shape of the rocket, we also note that exact details of the rocket's shape are of less importance for the problem of plasma-object interaction and the floating potential [Miloch et al., 2007]. The booms of the rocket would certainly modify the results to a certain degree [Miyake et al., 2013], but the cylindrical body of the rocket will dominate the plasma disturbances far away from the surface [Meyer-Vernet, 1976] and is used here as a first approximation. Moreover, for computational reasons we scale down the cylinder but maintain the characteristic ratios between the typical lengths in plasma: cylinder radius, Debye length, and electron/ion gyroradius, so as to reflect the conditions in the ionospheric F layer.

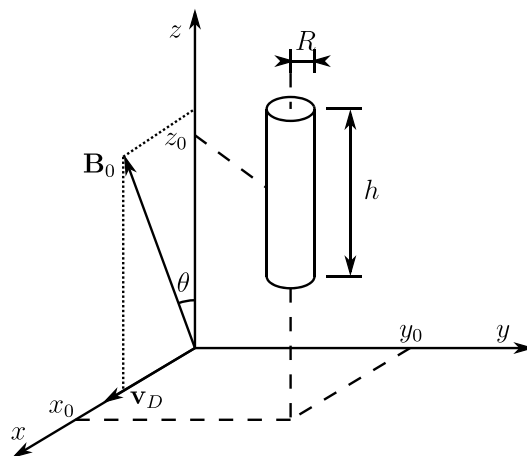


Figure 1. Simulation setup. R and h are the radius and height of the cylindric rocket, θ is the angle between the rocket axis and direction of the magnetic field, \mathbf{v}_D is the direction of the flow, (x_0, y_0, z_0) is the position of the center of the rocket.

We run a series of simulations where we change the angle between the rocket axis and the magnetic field θ , as defined in Figure 1 showing the schematics of the simulation setup and the flow speed v_D . The plasma parameters chosen for our simulations are listed in Table 1. Characteristic scales for the simulated species are derived in Table 2.

The simulations are run on a simulation box composed of a $128 \times 128 \times 128$ grid. The spatial step size is set to $\Delta r = 1.18\lambda_{De}$. This fulfills the spatial stability requirement $\Delta r < \pi\lambda_D$ [Birdsall and Langdon, 2004]. We use 32 superparticles per species per cell (on average) rather than the full $2 \cdot 10^5$ true particles per species per cell given in Table 1. Hence, each superelectron has a much greater mass and charge, which corresponds to that of 6250 true electrons. Since the charge-to-mass ratio is unaffected, the particle acceleration due to the Lorentz force and thus the characteristic scales for electrons listed in Table 2 are invariant of this transformation. The ion mass is reduced such that the ion-electron mass ratio m_i/m_e is 500 rather than the real proton-to-electron value of 1836. This difference is even larger for oxygen plasma which is the dominant specie in the ionospheric *F* layer. The reduced mass ratio has the effect of decreasing the ion plasma and cyclotron periods, as well as the gyroradius (but not the Debye length). The decreased characteristic timescales of the ions means that the simulations will reach steady state earlier, lowering the cost of the simulations [Miloch et al., 2007; Birdsall and Langdon, 2004]. We emphasize that Table 2 lists the characteristic scales for the simulated (reduced mass) ions.

The time step used is $\Delta t = 0.08\omega_{pe}^{-1}$ and 10,000 time steps are computed before extracting the electric potential at the last time instant. The total simulation time is then $T = 37.6\omega_{pi}^{-1}$ indicating that steady state is reached. Clearly, the temporal stability requirement $\omega_{pe}\Delta t < 1.62$ [Birdsall and Langdon, 2004] for warm plasma is satisfied, and $\Delta r/\Delta t = 14.8v_{th,e}$, where $v_{th,e}$ is the electron thermal velocity. Thus, the Courant-Friedrichs-Lowy condition is satisfied for the vast majority of the particles in the Maxwellian velocity distribution.

Notice from Table 2 that the ion gyromotion appears at much greater spatial scales than that of the rocket considered herein, and, as such, the ions (as opposed to the electrons) are considered weakly magnetized.

As we can see from the schematics of the simulation domain in Figure 1, the cylinder is centered inside the domain and aligned along the z axis. The particles are drifting in the x direction with speed $v_D = Mc$, where

Table 1. Simulation Parameters

Parameter		Value
Electron density	n_e	$2.0 \cdot 10^5 \text{ cm}^{-3}$
Ion density	n_i	$2.0 \cdot 10^5 \text{ cm}^{-3}$
Electron temperature	T_e	3000 K
Ion temperature	T_i	2000 K
Magnetic field	B_0	50 μT

Table 2. Characteristic Scales of the Simulated Species

Parameter	Electron	Ion ($s = e$)	Ion ($s = i$)
Debye length	λ_{Ds}	0.85 cm	0.69 cm
Plasma period	$2\pi\omega_{ps}^{-1}$	0.25 μ s	5.56 μ s
Cyclotron period	$2\pi\omega_{cs}^{-1}$	0.71 μ s	357 μ s
Gyroradius at thermal speed	r_s	2.43 cm	44.3 cm

M is the Mach number [Bar-Meir, 2007], and $c_s = \sqrt{k_b(T_e + T_i)/m_i}$ is the acoustic speed. Particles may leave the domain, but new particles are also injected at the boundaries with an influx according to the drifting Maxwellian distribution. The magnetic field vector \mathbf{B}_0 is in the xz plane with an angle θ with respect to the z axis. In order to study the influence of the orientation of the magnetic field for both subsonic and supersonic flows, simulations were carried out for three Mach numbers of 0.6, 1.2, and 2.4 and for angles θ of 0° , 45° , and 90° . In addition, simulations without external magnetic field were also carried out to provide a reference for comparison with studies neglecting the magnetic field.

In the rocket's frame of reference, the drift velocity and the magnetic field will induce a constant electric field \mathbf{E}_0 in order to satisfy the relation for the $\mathbf{E}_0 \times \mathbf{B}_0$ drift [Pécseli H. L., 2013]

$$\mathbf{v}_D = \frac{\mathbf{E}_0 \times \mathbf{B}_0}{|\mathbf{B}_0|^2}, \quad \Rightarrow \quad \mathbf{E}_0 = -|\mathbf{v}_D||\mathbf{B}_0| \cos \theta \hat{y},$$

where \hat{y} is the unit vector in the y direction. Thus, the total electric potential Φ in the simulations will have a background component Φ_0 with a constant gradient, which is defined as

$$\begin{aligned} \mathbf{E}_0 &= -\nabla\Phi_0, \\ \Rightarrow \Phi_0(y) &= -|\mathbf{E}_0|(y - y_0) = |\mathbf{v}_D||\mathbf{B}_0|(y - y_0) \cos \theta, \end{aligned}$$

where the integration constant is arbitrarily chosen such that $\Phi_0(y_0) = 0$. Since this component would exist even in the absence of the object, the potential can be decomposed into one part solely due to the $\mathbf{E}_0 \times \mathbf{B}_0$ drift (Φ_0) and one due to the disturbances caused by the object (Φ'):

$$\Phi = \Phi_0 + \Phi'.$$

In order to study the disturbances due to the object, Φ_0 is subtracted from the simulation results before analyzing the data.

Due to the reduced ion-to-electron mass ratio, as well as the scaled rocket and plasma parameters, as compared to the ionospheric F layer, the obtained results should be interpreted carefully in a quantitative sense. However, since the characteristic ratios are maintained, we can still address the fundamental processes of the object-plasma interactions in a qualitative manner.

3. Numerical Results

For plasma parameters given in the numerical setup section, we carried out a set of simulations for different orientations of the rocket with respect to the background magnetic field \mathbf{B}_0 . The angle θ between the rocket axis and \mathbf{B}_0 may reflect the geographical latitude: a spinning rocket will be close to parallel orientation ($\theta \approx 0^\circ$) in the polar regions and nearly perpendicular ($\theta \approx 90^\circ$) at the equator. We first present results for the supersonic flow and continue with the subsonic flow of plasma around the rocket.

3.1. Supersonic Flow

Supersonic plasma flow around the rocket gives rise to a clear wake in the potential and density downstream. The wake structure in the electric potential behind the rocket is shown in Figure 2 for $\theta = 0^\circ$ for two cases: $M = 1.2$ and $M = 2.4$. The potential distribution is shown in the xy and xz planes, where the rocket axis is along the z direction.

The wake downstream of the rocket is characterized by an extended negative potential in the downstream direction. We define the wake size as the smallest rectangular box (of length w_x , width w_y , and height w_z)

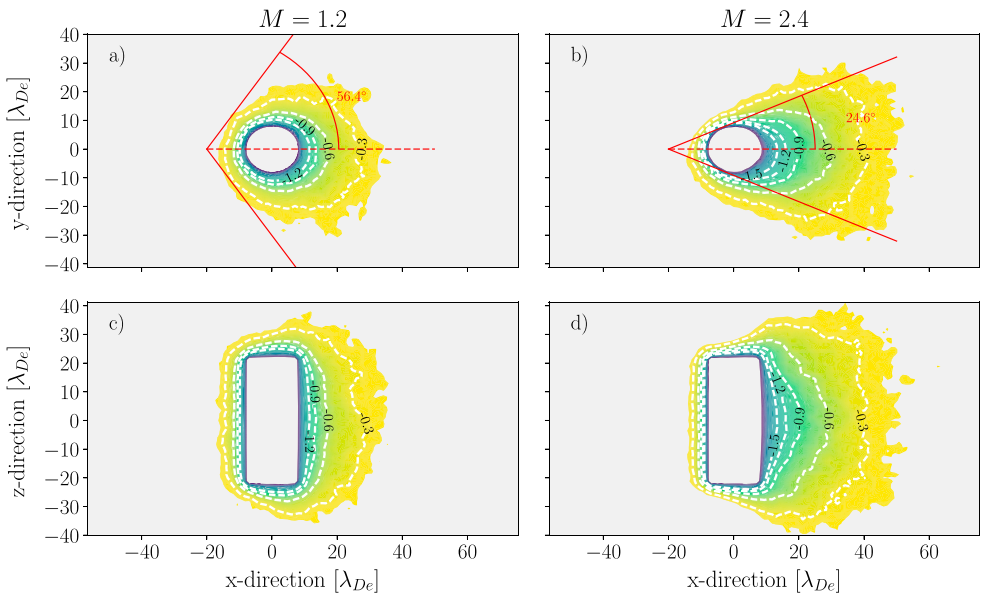


Figure 2. The normalized electric potential $e\Phi'/k_B T_e$ around the rocket for two supersonic cases with (left) $M = 1.2$ and (right) $M = 2.4$ for $\theta = 0^\circ$ (rocket aligned with \mathbf{B}_0). (a, b) The cuts at $z = 0$ in the xy plane, (c, d) the cuts at $y = 0$ in the xz plane. The flow is in the positive x direction. Only small potential variations $e\Phi'/k_B T_e \in (-1.2, -0.2)$ with respect to background plasma potential are colored for clarity. A Mach-like cone behind the rocket is clear for $M = 2.4$.

which encapsulates the region where $|\Phi'| < 0.2k_B T_e/e$. Under stationary conditions this would correspond to $w_x = w_y = w_z \approx 2\lambda_{De}$, indicating symmetric screening of the object, and where the total Debye length is used. In streaming plasmas, it is however natural to use the electron Debye length λ_{De} as the effective shielding length [Ludwig et al., 2012] and we use λ_{De} for presenting the results in the following. For $M = 1.2$ the extent of the wake is $w_x = 26\lambda_{De}$, $w_y = 51\lambda_{De}$, and $w_z = 64\lambda_{De}$. The wake gets bigger for $M = 2.4$ with $w_x = 40\lambda_{De}$, $w_y = 55\lambda_{De}$, and $w_z = 73\lambda_{De}$. Thus, doubling the speed of the supersonic flow increases the wake by about 40% in the x direction, and 9% and 15% in the y and z directions, respectively. This corresponds to increasing the wake volume by approximately 80%. The wake structure for different orientation θ of the magnetic field are visually similar to those displayed in Figure 2, and we choose not to present them in this paper.

For $M = 2.4$, a clear Mach-like cone in the potential distribution is visible downstream of the rocket, while it is less pronounced for $M = 1.2$. To compare with the theoretical half angle of the Mach cone, given by $\mu = \arcsin(1/M)$ [Bar-Meir, 2007], this half angle is drawn atop of the potential distribution in Figure 2 (red lines). There is a rather good agreement between the numerical results and theoretical expectations. However, one can observe an unexpected asymmetry in the wake along the x axis: the wake is slightly tilted in the xy plane as it extends farther toward the negative y direction.

The negative potential structure in the wake is reflected in the electron and ion densities, which are presented in Figure 3. The strong density depletion just downstream of the rocket, where the densities are close to zero, is gradually filled in, but it extends as far as $40\lambda_{De}$ downstream. Thus, the plasma density is significantly modified in the vicinity of the rocket, with depletion up to 50% of the background density at a distance of approximately $20\lambda_{De}$. Since the electric potential is directly related to the electron and ion densities $\nabla^2\Phi \propto (n_e - n_i)$, we will, in the remainder of this section, mainly present the results for the electric potential and omit the results of the simulations for the ion and electron densities.

To gain a detailed insight into the wake structure, we have in Figure 4 displayed the electric potential for $M = 1.2$ for different θ , behind the rocket along the (a) z axis and (b) y axis, and (c) along the x axis through the rocket body. The figure reveals an interesting feature about the floating potential Φ_f of the rocket in magnetized plasma: it is at its lowest value (most negative) in the absence of any magnetic field. In the presence of magnetic field, as the angle θ between the axis of the rocket and the magnetic field decreases, Φ_f becomes less negative, and it reaches the maximum (i.e., the least negative value) for $\theta = 0^\circ$. This is also visible in the potential of the wake, where it is most pronounced and has the largest extent for the case without the magnetic field.

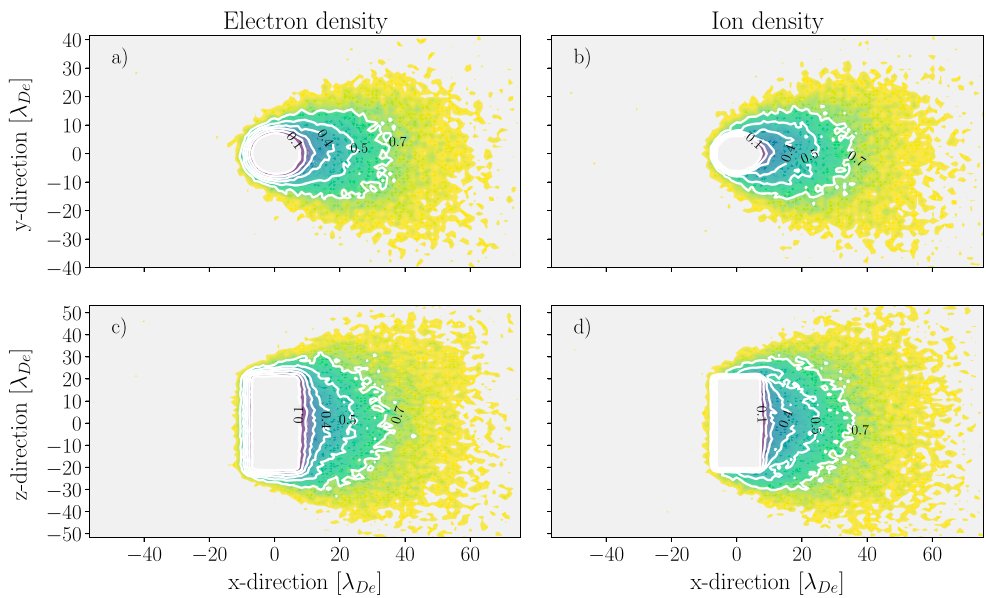


Figure 3. Normalized electron (left) and ion (right) densities around the rocket for the supersonic case where the $M = 2.4$ and $\theta = 0^\circ$. (a, b) The cuts at $z = 0$ in the xy plane, (c, d) the cuts at $y = 0$ in the xz plane. The plasma flow is in the positive x direction, corresponding to the rocket moving toward the negative x -direction.

The anisotropic disturbance of plasma will influence measurements at a certain distance from the surface, such as those performed by instruments on rocket booms. To evaluate these disturbances, we have in Figure 5 plotted the electric potential in the xy plane at $z = 0$ corresponding to a certain distance from the rocket for (a) $M = 1.2$ and (b) $M = 2.4$. We choose the distance $d = 4.7\lambda_{De}$ from the surface. With this choice of d , we can probe the wake structure in a rather close distance from the rocket. In Figure 5, the angle 0° corresponds to the downstream direction. The increasing angle corresponds to counterclockwise direction in the xy plane, and angle 180° is related to the ram direction, i.e., antiparallel to the direction of the flow.

Figure 5 clearly shows that the electric potential has a spin-modulated structure around the rocket; the lowest value of the potential corresponds to the middle of the wake. As we move around toward the upstream

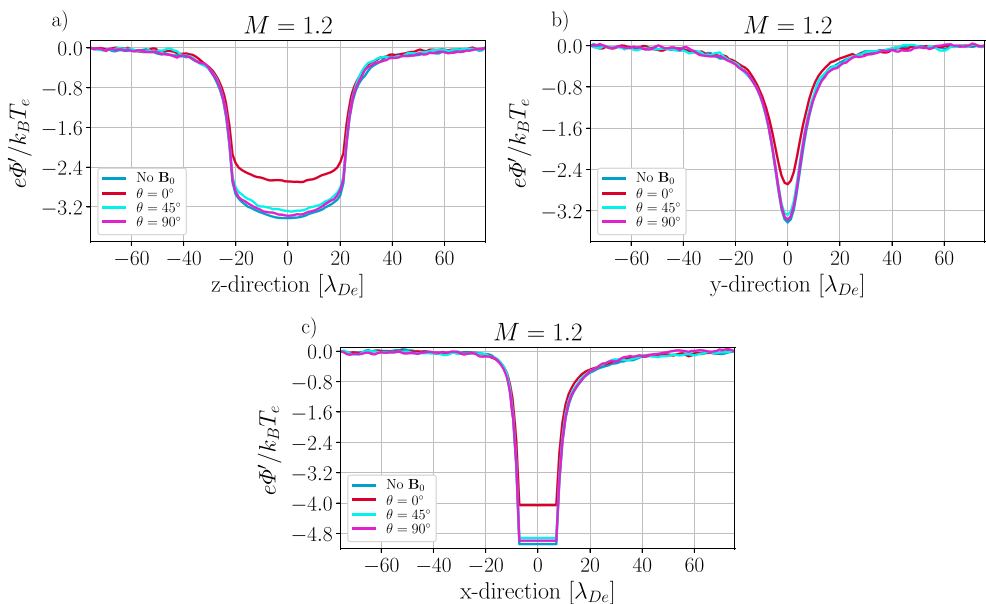


Figure 4. The electric potential along the (a) z axis ($x = 8.3\lambda_{De}$, $y = 0$), (b) y axis ($x = 8.3\lambda_{De}$, $z = 0$), and (c) x axis ($y = z = 0$).

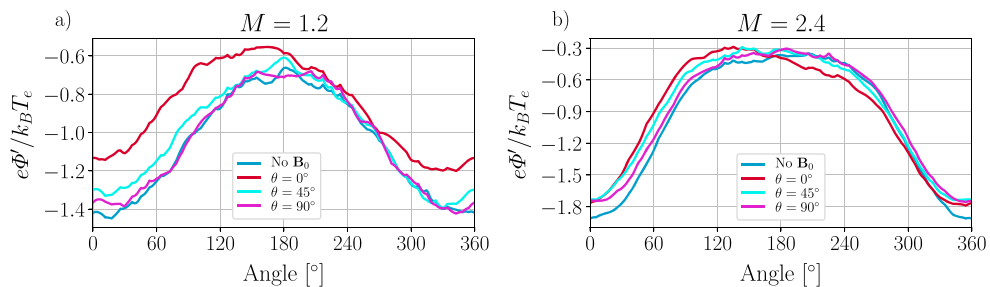


Figure 5. The electric potential along a circle at $z = 0$, with a distance $d = 4.7\lambda_{De}$ from the surface of the rocket for (a) $M = 1.2$ and (b) $M = 2.4$. An increased asymmetry in the wake potential can be observed for smaller θ .

direction, the potential increases, and its maximum value corresponds to the ram direction. In the ram direction it still corresponds to a potential drop with respect to the plasma reference potential (arbitrarily set to 0 V), indicating that the sheath effect is still visible at this point. This potential value can be related to the expected potential drop in the presheath which is about $\Delta\Phi' = 0.5k_B T_e/e$ [Lieberman and Lichtenberg, 2005].

For Mach number $M = 1.2$, the electric potential for the case without magnetic field is rather symmetric around the rocket. The disturbances observed in Figures 5a and 5b for this case can be related to the fluctuations in the potential distribution. However, when an external magnetic field \mathbf{B}_0 is included in the simulation, the situation changes: the $\theta = 90^\circ$ magnetic field case does not have any significant impact on the electric potential, but as θ decreases, the potential gradually increases, which is related to different Φ_{fl} , and at the same time it becomes asymmetric. Both minimum and maximum are slightly shifted with respect to the direction of the flow, and the potential slope is slightly steeper in the first half of the circle, which corresponds to $y > 0$. This shift seems plausible given the slight tilt of the wake presented in Figure 2a. The maximum shift in the electric potential around the rocket is found to be approximately 18° for the magnetic field parallel with the rocket, that is for $\theta = 0^\circ$.

For larger Mach number, $M = 2.4$, the angle $\theta = 90^\circ$ again does not lead to a significant change compared to the case without any magnetic field, see Figure 5b. The increase in the electric potential with decreasing θ is, however, less profound than the case with $M = 1.2$, reflecting that Φ_{fl} is less sensitive to θ in the fast flow. Likewise, the shift in the potential distribution is less pronounced, and the maximum shift occurs for $\theta = 0^\circ$ and is approximately 9° . In addition to the shift in the electric potential, we observe clear asymmetry in the slopes for the electric potential around the rocket. This shift might be related to the slight tilt in the wake presented in Figure 2: the electric potential increases faster when rotating from the wake center (angle 0° in Figure 5) toward positive y values, and slower when rotating toward negative y values.

In order to study how far the wake extends behind the rocket, and how the plasma is disturbed at larger distances, we have, in Figures 6a and 6b, displayed the potential along the z and y axes, for increasing distances from the rocket in the x direction (in the flow direction). Figure 6c shows, in addition, the electric potential around the rocket in the xy plane for increasing distances from the surface of the rocket. The data correspond to the case where the magnetic field is parallel to the axis of the rocket and flow is supersonic: $M = 1.2$ and $\theta = 0^\circ$. The corresponding figures for other cases are not displayed because of their overall similarity to the case presented here. As expected, the potential in the wake gets smaller with the increasing distance from the rocket, tending toward the plasma potential of 0 V. However, it is clear that a significant wake extends as far as $30\lambda_{De}$ behind the rocket. The potential disturbances at $d = 20\lambda_{De}$ for the circle taken around the rocket lead to variations $\Delta\Phi'$ of $0.25k_B T_e/e$.

Finally, the disturbance in the electron density, $\delta n_e = n_0 - n_e$, downstream of the rocket for the case of a parallel magnetic field is displayed in Figure 6d, which shows that δn_e decreases more rapidly for slower plasma flow.

3.2. Subsonic Flow

As the rocket flight can also be subsonic with respect to the ionospheric plasma, we have also run simulations for a case with $M = 0.6$. In Figures 7a and 7b the potential distribution around the rocket is shown in the xy and xz planes. It is evident that the wake has diminished and is not clear in the potential distribution. However, one can observe the asymmetry in the potential corresponding to asymmetric sheath around the object.

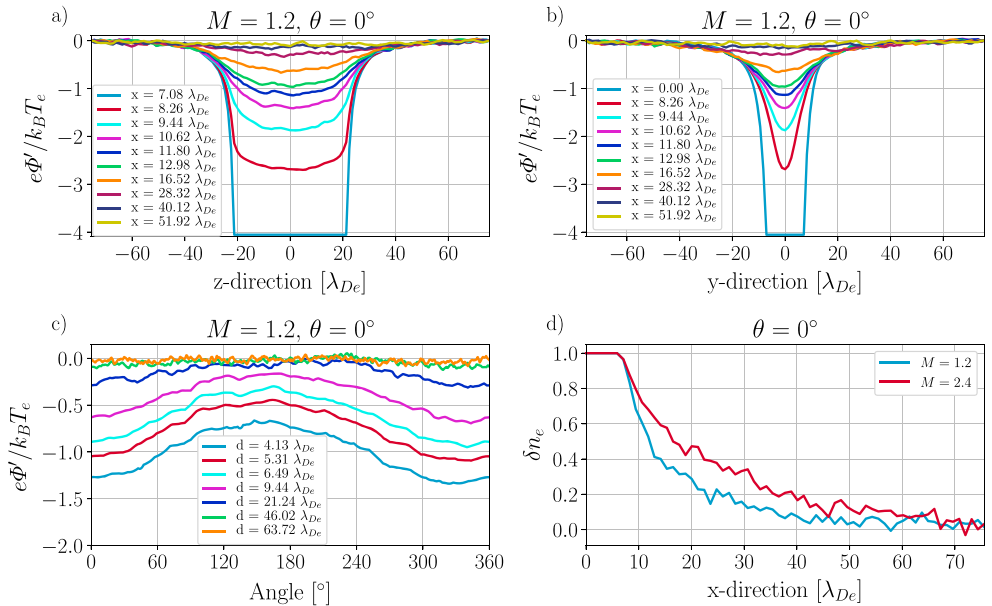


Figure 6. The electric potential behind the rocket, along the (a) z axis ($y = 0$) and (b) y axis ($z = 0$) for increasing distances from the rocket along the x axis. (c) The electric potential in xy plane ($z = 0$) for increasing distances from the surface of the surface d . Again, note the asymmetry in the potential wake in this case. (d) The disturbances in the electron density downstream of the rocket.

This asymmetry can extend to a certain distance, and with the measure introduced for the supersonic case, we obtain: $w_x = 20\lambda_{De}$, $w_y = 46\lambda_{De}$, and $w_z = 61\lambda_{De}$.

The wakes in the densities of ions and electrons exhibit similar behavior to the electric potential (data not shown here). To see how the disturbances in the densities change compared to the supersonic cases, we have, in Figures 7c and 7d, displayed the disturbances in the ion and electron densities, respectively. Al'pert *et al.* [1965] have shown analytically that the disturbance in the ion density, $\delta n_i = n_0 - n_i$, in the wake region, decreases with increasing distance from the rocket as $\delta n_i \sim x^{-1}$ and that the disturbance in the electron

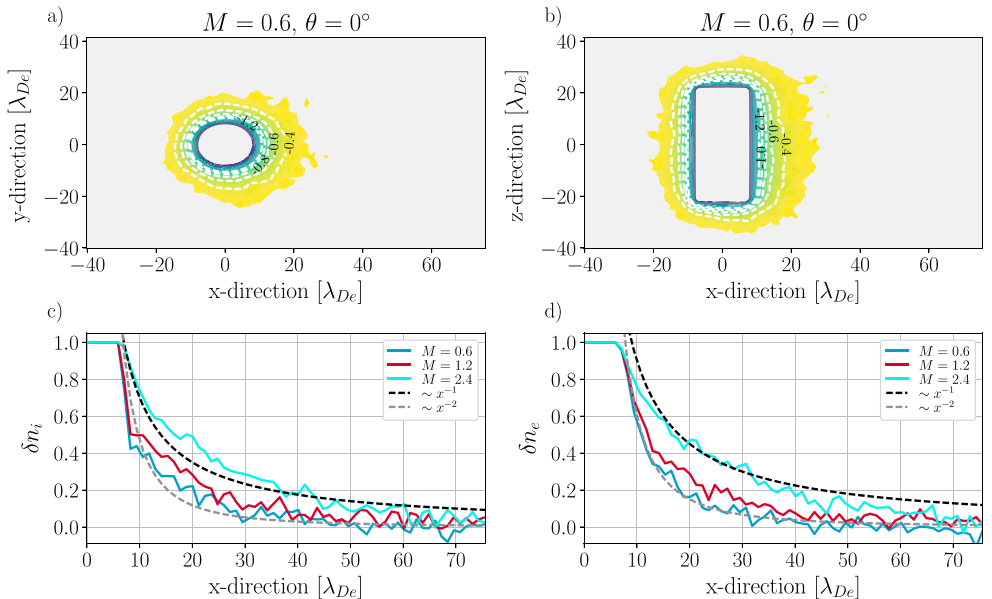


Figure 7. The electric potential around the rocket in (a) xy plane and (b) xz plane for the subsonic case where the $M = 0.6$ and $\theta = 0^\circ$. The (c) ion and (d) electron disturbances behind the rocket for the case $\theta = 0^\circ$ for different flow velocities (solid lines) together with theoretical fits (dashed lines).

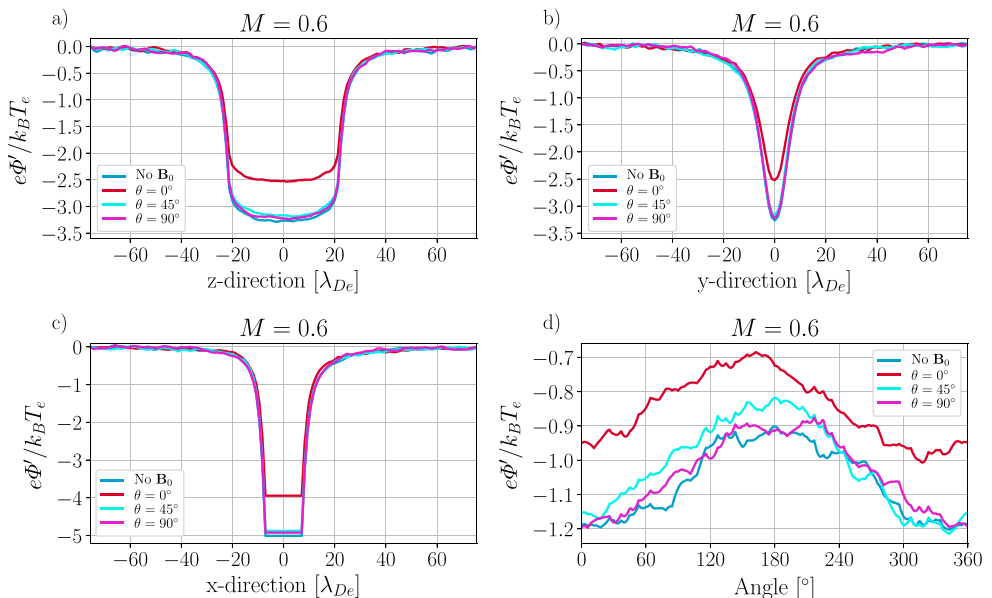


Figure 8. The electric potential along the (a) z axis ($x = 8.3\lambda_{De}$, $y = 0$), (b) y axis ($x = 8.3\lambda_{De}$, $z = 0$), and (c) x axis ($y = z = 0$). (d) The electric potential along a circle at $z = 0$, with a distance $d = 4.7\lambda_{De}$ from the surface of the rocket. Note the asymmetry in the wake distribution, where both the slopes and also the position of the extreme are increasingly shifted for smaller θ .

density δn_e decreases faster and scales as $\delta n_e \sim x^{-2}$. For the sake of comparison, we have, in Figures 7c and 7d, also displayed the curves for $\sim x^{-1}$ and $\sim x^{-2}$. Our simulations show that for $M = 0.6$ the disturbances in the ion and electron densities scale close to x^{-2} . As we increase the Mach number, the disturbances close to rocket, decrease slower, i.e., they scale closer to x^{-1} . However, farther downstream, both δn_i and δn_e scale close to x^{-2} .

In Figure 8, the potential profiles for different θ are plotted just as in Figures 4 and 5. Similar to the supersonic case, the highest (most negative) floating potential Φ_f is obtained in the absence of any magnetic field. In the presence of the magnetic field, Φ_f gets less negative and depends on the angle between the magnetic field and the axis of the rocket, being lowest (least negative) for $\theta = 0^\circ$. The potential is, in general, less negative than for the supersonic flow.

From Figure 8d, which shows the electric potential at $d = 4.7\lambda_{De}$ from the surface, it follows that the potential variations are related to the orientation of the magnetic field. For $\theta = 90^\circ$, the wake is symmetric with respect to the flow direction. With decreasing θ , the electric potential steadily rises and its maximum shifts to the left (in the positive y direction). Again, the maximum shift in the electric potential corresponds to the parallel magnetic field case with respect to the rocket $\theta = 0^\circ$, and it is approximately 36° .

4. Discussion

4.1. The Sheath and the Wake Structure

A sounding rocket immersed in a plasma gives rise to a sheath forming around it. Consequently, the ion and electron densities are disturbed, and the quasi-neutrality condition is locally broken. The resulting electric field will affect the dynamics of electrons and ions. In addition, the plasma dynamics is influenced by the magnetic field. Finally, the sounding rocket forms an obstacle for the stream plasma and a wake is formed.

To set the context for the results presented in the previous section, let us first look at the electron and ion dynamics in the simulated system. In our study, the electrons have a much greater thermal velocity than drift velocity. For the supersonic plasma flow of $M = 2.4$, in the vicinity of the rocket, the thermal energy of electrons, $k_B T_e \approx 0.26$ eV, exceeds many times their kinetic drift energy due to the drift velocity, $m_e v_D^2/2 \approx 1.59 \cdot 10^{-3}$ eV. For ions the situation is opposite: their kinetic energy due to the drift velocity, $m_i v_D^2/2 \approx 0.80$ eV, is larger than their thermal energy $k_B T_i \approx 0.17$ eV. Furthermore, for ions the potential energy in the sheath is approximately on the order of their thermal energy. Thus, it is expected that

the structure of the wake is to a large degree controlled by the streaming ions, while the electrons will be mostly providing neutralizing background. However, since the simulated electrons are strongly magnetized, the effect of the magnetic field on their dynamics needs to be considered, and it will be discussed in the following.

For the ionospheric conditions that we are interested in, the Debye radius is much smaller than the characteristic size of the rocket. Furthermore, the gyroradius of ions is larger than the radius of the rocket, thus, while being in the sheath, ions are minimally affected by the presence of the magnetic field. On the other hand, the gyroradius of electrons is smaller than the radius of the rocket, and therefore, the presence of the magnetic field has an important impact on their motion toward the surface of the rocket.

Figures 2, 5, and 8d, revealed an asymmetric potential profile in the azimuthal direction, where the electric potential is somewhat shifted in the direction of negative y axis. The asymmetry is most profound in the case of a parallel magnetic field. As the angle θ (between the magnetic field and the axis of the rocket) increases, the asymmetry gradually fades away. This asymmetry has previously been predicted in analytical works by other authors [Grabowski and Fischer, 1974] only for the case of a parallel magnetic field. Our numerical study supports the presence of the suggested asymmetry, and we have also seen that it exists for other orientations of the magnetic field, with the exception of when the drift velocity is parallel to the magnetic field.

The asymmetry in the electric potential seems to be caused by the fact that there are more electrons in the region $y < 0$ than there are in the region $y > 0$, when the rocket is centered at $(x, y, z) = (0, 0, 0)$. Since the rocket is negatively charged, the electric field is directed toward the surface of the rocket. Electrons incident on the rocket will thus experience an $\mathbf{E} \times \mathbf{B}_0$ drift, which forces them to move perpendicular to both the \mathbf{E} and \mathbf{B}_0 fields. For this reason the electrons will move toward the $y < 0$ region [Grabowski and Fischer, 1974].

In the absence of any electric or magnetic fields, plasma particles move around freely with their given thermal and drift velocities. With a uniform magnetic field, the motion of electrons and ions in the directions normal to the magnetic field will be restricted; i.e., ions and electrons can move freely only in the direction parallel to the magnetic field. Thus, the ions and electrons will gyrate, with the gyrofrequency $\omega_{cs} = eB_0/m_s$, in a plane perpendicular to the direction of the magnetic field, given that they initially have a finite thermal velocity component normal to the magnetic field. The effect of the magnetic field on the motion of the particles is significant only over time interval $\Delta t > 2\pi/\omega_{cs}$. During this time the gyrocenter has moved a distance $\Delta r \sim 2\pi v_D/\omega_{cs}$. Since the gyroradius is much larger for ions than for electrons, the effect of the magnetic field on ions is small at distances that are comparable to the rocket diameter. However, at distances $\Delta r > 2\pi v_D/\omega_{cs}$ the effect of the magnetic field on the ions will be essential.

As we have seen from Figure 6, the disturbances in the electric potential, and therefore in the plasma density, may extend as far as $30\lambda_{De}$ downstream of the surface of the rocket. These disturbances will have an important impact on the in situ measurements. Such disturbances have been reported in sounding rocket experiments [Meyer-Vernet, 1976; Svenes et al., 1990]. Thus, to ensure that we have reliable measurements of the ionospheric plasma, it is important to account for the disturbances due to the effects of the rocket wake and also due to the magnetic field.

To demonstrate these effects, the numerical results that have been presented in this paper can be related to experimental data. In Figure 9, we present an example of the data from the ICI-3 sounding rocket experiment [Spicher et al., 2016]. For clarity we show only 2 s of the approximately 10 min long flight. The ionospheric plasma conditions during the rocket flight were similar to plasma parameters considered in this numerical study. The ICI-3 rocket has four 87 cm long booms mounted at the tip of the rocket payload. On these booms two different sets of probe systems are mounted; two electric field probes (two sets of two spherical probes) at the tip of the booms, eight Langmuir probes mounted on the booms halfway between the tip and the rocket payload. The data shown in Figure 9 are from one of the electric field probes and two of the cylindrical Langmuir probes. More details on the rocket flight conditions and design can be found in Spicher et al. [2016].

The convective electric field is perpendicular to the wake in the rocket frame of reference. This can be used for determining the wake position. The vertical lines in Figure 9 thus represent when the double probe is parallel to the convective electric field. The fixed-bias Langmuir probes, NLP4 and NLP8, were mounted on booms perpendicular to the double probe DC1 on opposite sides of the rocket. Hence, when DC1 is parallel to the electric field NLP4 should be in the wake, and NLP8 in upstream and unperturbed conditions. As is seen in Figure 9, it is evident that the signal is spin modulated and that the current measurements are influenced by the wake

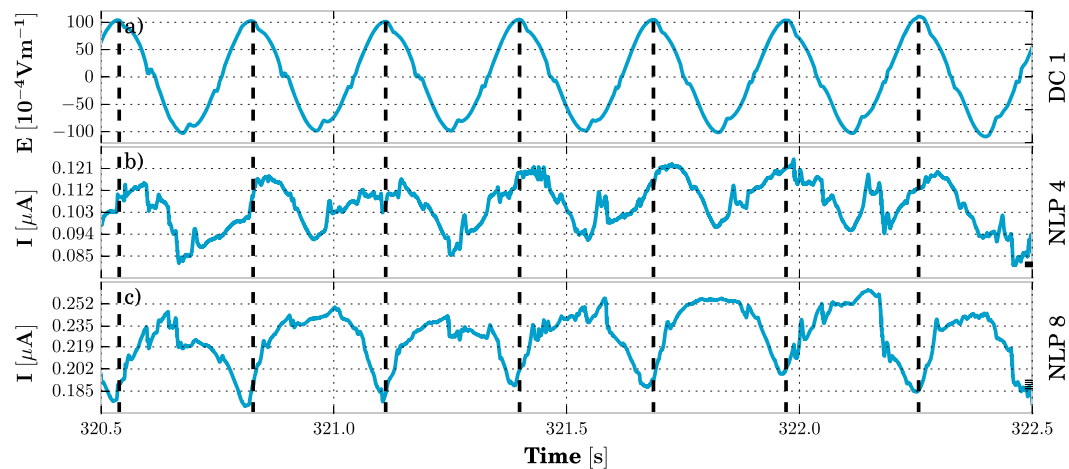


Figure 9. Example of data from ICI-3 rocket experiment during 2 s of the flight. The rocket is spin stabilized and therefore the electric field measurements are modulated in time by the spin of the rocket. (a) Data from double probe electric field experiment, (b, c) currents to Langmuir probes. The vertical lines indicate double probe being parallel to the direction of the electric field, showcasing that NLP4 (Figure 9b) is in the wake of the rocket and NLP8 (Figure 9c) is in the upstream, unperturbed, condition. Ephemeris information from the ICI-3 rocket: velocity: ~ 1 km/s, altitude: 354.5 km, magnetic field: latitude: 1.63° , longitude: 82.63° , MLT: 10–11. The magnetic field strength is roughly equal to the parameter value used in the simulations.

potential being lower downstream. Since NLP currents are related to the electron density, and the electron density to electric potential, we can relate these in situ measurements to simulation results. Both experiment and simulation show similar magnitude of rarefaction. Therefore, care should be taken when analyzing experimental results in order to properly account for wake effects. The Langmuir probes are approximately $45\lambda_D$ from the rocket, where the density rarefaction (as reflected by currents to the probes), as seen from Figure 6d, should be between 15% and 20%, which is roughly what the data in Figure 9 show. Hence, simulation and experimental data show qualitative agreement.

4.2. Floating Potential

The floating potential of the rocket depends on the electron and ion fluxes to its surface. In order to understand the simulation results displayed in Figures 4 and 8, showing how the rockets floating potential change depending on the magnetic field orientation, we have in Figures 10a and 10b displayed the time evolution of the number of electrons and ions hitting the surface of the rocket for different orientation of the magnetic field for $M = 1.2$. The main observation here is that the electron influx for a parallel magnetic field drops more rapidly compared to other orientations of the magnetic field, and also the ion influx is clearly lower for this particular case. This feature is also reflected in Figure 10c, showing the cumulative difference between the number of electrons and ions hitting the surface of the rocket, where a positive influx means that the electron flux is dominant. The floating potential, shown in Figure 10d, is determined by the influx onto the surface of the rocket, and therefore, its time evolution reflects that of the cumulative difference. We note that the results for the other drift velocities are similar.

As we have seen in Figures 10a and 10b, the effect of the magnetic field on the floating potential seems to be related to the electron influx on the rocket. Electrons are magnetized and will gyrate in the plane perpendicular to the magnetic field with a guiding center that will move at the drift velocity. But at the same time, they will continue to move freely along the magnetic field. Their thermal velocity is much larger than the drift velocity, which implies that for $\theta = 90^\circ$, i.e., magnetic field perpendicular to the rocket axis, the electron current to the side surface of the rocket will be determined by the electron thermal velocity $v_{th,e}$. With decreasing θ , the electron flux to the surface will be a combination of the flux determined by $v_{th,e}$ and flux given by the drift velocity. However, due to tilted magnetic field lines, the effective electron flux to the side surface, determined by $v_{th,e}$ will change as $\sin \theta$, and will be negligible for $\theta = 0^\circ$, for magnetic field aligned with the rocket axis. For that orientation the flux to the side surface is solely determined by the drift velocity, which is much smaller than the electron thermal velocity. This decrease of electron flux to the side surface with decreasing θ can explain less negative floating potential for parallel orientation of the magnetic field.

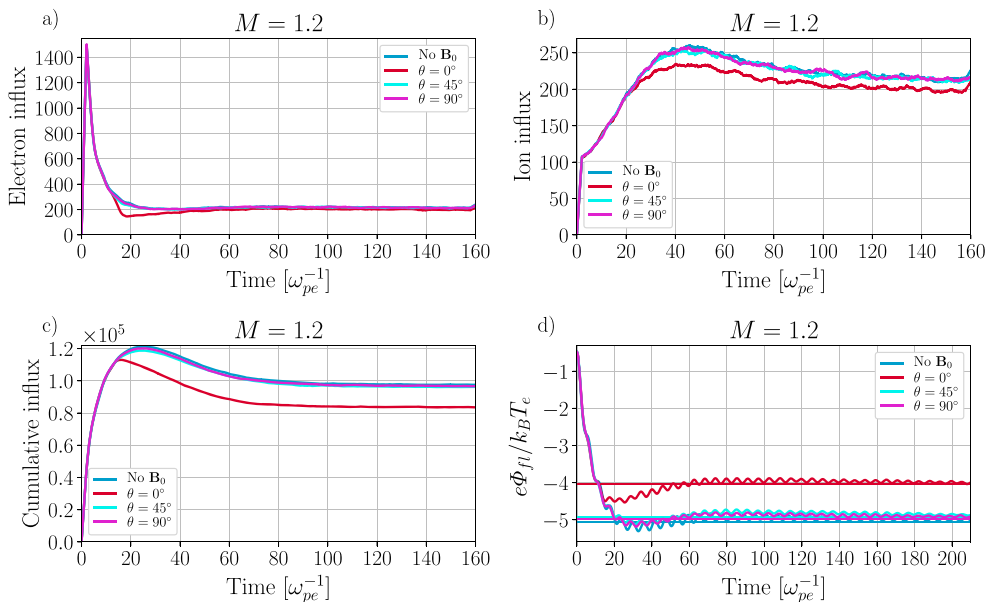


Figure 10. The time evolution of the number of the (a) electron and (b) ion fluxes to the rocket surface for different orientations of the magnetic field. (c) The time evolution of the cumulative net flux (difference between electron and ion fluxes). (d) The corresponding time evolution of the floating potential. Horizontal lines indicate the convergence of the floating potential. The frequency of oscillations in the floating potential is approximately the ion plasma frequency $\omega_{pi} \sim 1.8 \cdot 10^5$ Hz.

On the other hand, the top and bottom surfaces of the simulated rocket will experience different effects. The electron current to those surfaces will be determined by $v_{th,e}$ for $\theta = 0^\circ$, i.e., magnetic field parallel to the rocket axis. Since the flow is in the direction perpendicular to the rocket axis and these surfaces are parallel to the flow, for $\theta = 90^\circ$ the current to the top and bottom surfaces will not change significantly, and again high thermal velocity of electrons will provide significant flux also in this case. However, since the side surface of the rocket is much larger than the top/bottom sides, the variations in the flux to the side surface will dominate the net current to the rocket and control floating potential. Note that in our simulated system ions can be considered as unmagnetized with respect to the rocket body, and their flux will not change with θ . In our simulations we could not differentiate between fluxes to different parts of the body, and such a study should be performed in future to assess this issue in detail.

The largest reduction in the total electron influx corresponds to the parallel magnetic field, which results in the largest decrease in the negative floating potential of the rocket. This is in agreement with *Marchand* [2012]: his simulation results for a spherical object in the presence of a magnetic field perpendicular to the plasma flow, i.e., $\theta = 0^\circ$, show that the presence of the magnetic field makes the floating potential less negative. In our work we have shown that compared with the case without magnetic field, the floating potential is less negative not only in the presence of a parallel magnetic field but also for other orientations of the magnetic field. Furthermore, the highest value (least negative) of the floating potential corresponds to the parallel magnetic field.

Similar results for the electric potential around a cylindrical object have been found theoretically by *Lafon* [1973], where it was shown that in the presence of a uniform and parallel magnetic field the electric potential should become less negative. The electrostatic theory of the effect of the magnetic field, its strength and orientation, on the floating potential of a cylindrical object was presented by *Laframboise and Rubinstein* [1976]. Based on that theory, the electric current into the cylindrical object decreases as the angle between the magnetic field and the axis of the object decreases. In accordance with the analytical study of *Laframboise and Rubinstein* [1976], the simulation results presented in this work show that the presence of a parallel magnetic field also makes the floating potential less negative. As the angle increases, the magnetic field will have less impact on the floating potential. In contrast to the work by *Meyer-Vernet* [1976], where it was concluded that, for ionospheric conditions, the effect of the magnetic field and its orientation on the current modulations

measured by Langmuir probes is negligible, our simulation results clearly demonstrate how the electric potential is changed due to the orientation of the magnetic field.

The change in the current to the rocket can be incorporated into analytical expressions. Taking for simplicity the case with a parallel magnetic field, i.e., $\theta = 0^\circ$, and assuming that the electron thermal velocity is much bigger than the drift velocity, the electron current is approximately given by equation (6). On the other hand, in the case of unmagnetized plasma the electron current is given by equation (3). Since the thermal velocity of the ions is smaller than the drift velocity, and they are weakly magnetized, we can assume that the ion current is approximately given by equation (5). Floating potential is obtained when the net current is zero. Thus, for the unmagnetized case, equating equations (3) and (5), yields

$$\left(\frac{\sqrt{\pi} \bar{v}_e}{\bar{v}_i} \right)^2 e^{\frac{-2e|\Phi_{fl}|}{k_B T_e}} - \frac{e\Phi_{fl}}{k_B T_i} = \frac{1}{2} + \frac{m_i v_D^2}{2k_B T_i}, \quad (9)$$

where we have assumed that the plasma potential is zero, i.e., $\Phi_{pl} = 0$. Similarly, for the magnetized case (assuming a parallel magnetic field), equating equations (5) and (6), we obtain

$$\left(\frac{\sqrt{\pi} \bar{v}_e}{\bar{v}_i} \right)^2 \left[\frac{1}{2} + \frac{1}{2} \left(\frac{8e|\Phi_{fl,B}|}{m_e \omega_{ce}^2 R^2} \right)^{\frac{1}{2}} + \frac{k_B T_e}{m_e \omega_{ce}^2 R^2} \right]^2 - \frac{e\Phi_{fl,B}}{k_B T_i} = \frac{1}{2} + \frac{m_i v_D^2}{2k_B T_i}. \quad (10)$$

We notice that the right-hand side of equations (9) and (10) are identical, thus

$$\frac{e\Phi_{fl}}{k_B T_i} - \frac{e\Phi_{fl,B}}{k_B T_i} = \left(\frac{\sqrt{\pi} \bar{v}_e}{\bar{v}_i} \right)^2 \left\{ e^{\frac{-2e|\Phi_{fl}|}{k_B T_e}} - \left[\frac{1}{2} + \frac{1}{2} \left(\frac{8e|\Phi_{fl,B}|}{m_e \omega_{ce}^2 R^2} \right)^{\frac{1}{2}} + \frac{k_B T_e}{m_e \omega_{ce}^2 R^2} \right]^2 \right\}. \quad (11)$$

For the parameters considered in this paper

$$\frac{k_B T_e}{m_e \omega_{ce}^2 R^2} > 1,$$

therefore, the right-hand side of equation (11) is less than zero, i.e.,

$$\frac{e\Phi_{fl}}{k_B T_i} - \frac{e\Phi_{fl,B}}{k_B T_i} < 0,$$

which means

$$|\Phi_{fl,B}| < |\Phi_{fl}|, \quad (12)$$

indicating that the effect of the magnetic field is to decrease the floating potential, i.e., less negative floating potential. This is indeed what we observe in the PIC simulation results.

5. Summary

In this paper we have, through extensive numerical PIC simulations, studied the charging of a cylindrical rocket in subsonic and supersonic weakly magnetized plasma flows and investigated the resulting wake formation. We have considered a uniform, static external magnetic field at a certain angle with respect to the rocket axis. The ionospheric plasma condition in this work correspond to fully magnetized electrons and weakly magnetized ions. Due to the greater mobility of electrons, the rocket will typically be negatively charged, and since the Debye length is much smaller than the radius of the rocket, the electrostatic sheath is thin with respect to the size of the rocket. For these conditions, we have demonstrated that the potential on the rocket and the wake structure depend on the orientation of the magnetic field with respect to the rocket axis. A magnetic field perpendicular to the rocket axis and at the same time parallel to the direction of the plasma flow has a minimal effect on the floating potential as compared to the unmagnetized case. As the angle between the magnetic field and the flow direction increases and consequently the magnetic field gets more aligned with the rocket axis, the floating potential becomes less negative. The least negative values of the floating potential correspond to a magnetic field parallel to the rocket axis (i.e., perpendicular to the flow).

In the presence of a magnetic field, the wake gets asymmetric in the azimuthal direction and it extends to distances of more than 30 electron Debye lengths. The extent of the wake and the plasma disturbances around

the rocket are analyzed for different flow regimes, and a quantitative agreement with the sounding rocket measurements has been found. It follows that depending on the distance between the rocket surface and the instruments mounted on the rocket booms, the plasma disturbances will affect the in situ measurements. It is therefore crucial to account for the plasma perturbations and wakes caused by the rocket when interpreting data from in situ experiments.

Acknowledgments

This work is the result of the Japan-Norway Partnership on Space Science Simulations, funded by the Norwegian Center for International Cooperation in Education SiU, grants UTF-2014/10043 and UTF-2016-long-term/10054, and it is a part of the 4DSpace Strategic Research Initiative at the University of Oslo. This research is supported in part by the Research Council of Norway grant 240000. The sounding rocket has been supported by the Research Council of Norway grants 208006 and 230996. The simulation data presented in this paper are available at DOI:10.11582/2017.00008.

References

- Allen, J. E. (2012), On supersonic plasma flow around an obstacle, *J. Plasma Phys.*, 79(3), 315–319.
- Allen, J. E., B. M. Annaratone, and U. de Angelis (2000), On the orbital motion limited theory for a small body at floating potential in a Maxwellian plasma, *J. Plasma Phys.*, 63(4), 299–309.
- Al'pert, J. L., A. V. Gurevich, and L. P. Pitaevskii (1963), Effects produced by an artificial satellite rapidly moving in the ionosphere or in an interplanetary medium, *Sov. Phys. Uspekhi*, 6(1), 13–46.
- Al'pert, J. L., A. V. Gurevich, and L. P. Pitaevskii (1965), *Space Physics with Artificial Satellites*, Consultants Bureau, New York.
- Anderson, P. C. (2012), Characteristics of spacecraft charging in low Earth orbit, *J. Geophys. Res.*, 117, A07308, doi:10.1029/2011JA016875.
- Bar-Meir, G. (2007), Oblique shock, in *Fundamentals of Compressible Fluid Mechanics*, Potto Project NFP, Minneapolis, Minn. [Available at <http://web.iitd.ac.in/~prms/courses/mel7152008/text.pdf>]
- Bernstein, I. B., and I. N. Rabinowitz (1959), Theory of electrostatic probes in low-density plasma, *Phys. Fluids*, 2(2), 112–121.
- Birdsall, C. K., and A. B. Langdon (2004), *Plasma Physics via Computer Simulation*, CRC Press, Taylor & Francis Group, Boca Raton, Fla.
- Bohm, D., E. H. S. Burhop, and H. S. W. Massey (1949), *The Characteristics of Electrical Discharges in Magnetic Fields*, McGraw-Hill, New York.
- Boris, J. P. (1970), Relativistic plasma simulation-optimization of a hybrid code, in *Proceedings of the Fourth Conference on the Numerical Simulation of Plasmas*, pp. 3–67, Naval Res. Lab, Washington, D. C.
- Block, D., and W. J. Miloch (2014), Charging of multiple grains in subsonic and supersonic plasma flows, *Plasma Phys. Controlled Fusion*, 57(1), 14019.
- Brace, L. H. (1998), Langmuir probe measurements in the ionosphere, in *Measurement Techniques in Space Plasmas: Particles, Geophys. Monogr. Ser.*, vol. 102, edited by R. F. Pfaff, J. E. Borovsky, and D. T. Young, pp. 23–35, AGU, Washington, D. C.
- Brundin, C. L. (1963), Effects of charged particles on the motion of an earth satellite, *Am. Inst. Aeronaut. Astronaut. J.*, 1(11), 2529–2538.
- Chen, F. F. (1965), *Electric Probes*, chap. 4, pp. 113–200, Academic Press, New York.
- Chung, P. M., L. Talbot, and K. J. Touryan (1974), Part 2. Continuum probes, *Am. Inst. Aeronaut. Astronaut. J.*, 12(2), 144–154.
- Cohen, I. J., M. Widholm, M. R. Lessard, P. Riley, J. Heavisides, J. I. Moen, L. B. N. Clausen, and T. A. Bekkeng (2016), Rocket-borne measurements of electron temperature and density with the Electron Retarding Potential Analyzer instrument, *J. Geophys. Res. Space Physics*, 121, 6774–6782, doi:10.1002/2016JA022562.
- Comfort, R. H., C. R. Baugher, and C. R. Chappell (1982), Use of the thin sheath approximation for obtaining ion temperatures from the ISEE 1 limited aperture RPA, *J. Geophys. Res.*, 87(A7), 5109–5123.
- de Leeuw, J. H. (1967), *A brief introduction to ionospheric aerodynamics*.
- Endo, K., A. Kumamoto, and Y. Katoh (2015), Observation of wake-induced plasma waves around an ionospheric sounding rocket, *J. Geophys. Res. Space Physics*, 120, 5160–5175, doi:10.1002/2014JA020047.
- Escoubet, C. P., A. Pedersen, R. Schmidt, and P. A. Lindqvist (1997), Density in the magnetosphere inferred from ISEE 1 spacecraft potential, *J. Geophys. Res.*, 102(A8), 17595–17609.
- Fernandes, P. A., and K. A. Lynch (2016), Electrostatic analyzer measurements of ionospheric thermal ion populations, *J. Geophys. Res. Space Physics*, 121, 7316–7325, doi:10.1002/2016JA022582.
- Garrett, H. B. (1981), The charging of spacecraft surfaces, *Rev. Geophys.*, 19(577), 577–616.
- Grabowski, R., and T. Fischer (1974), Theoretical density distribution of plasma streaming around a cylinder, *Planet. Space Sci.*, 23, 287–304.
- Grard, R. J. (1973), Properties of the satellite photoelectron sheath derived from photoemission laboratory measurements, *J. Geophys. Res.*, 78(16), 2885–2906.
- Gringauz, K. I., and M. Kh. Zelikman (1957), Measurement of the concentration of positive ions along the orbit of an artificial satellite, *Usp. Fiz. Nauk*, 63, 239–252.
- Guio, P., W. J. Miloch, H. L. Pécseli, and J. Trulsen (2008), Patterns of sound radiation behind pointlike charged obstacles in plasma flows, *Phys. Rev. E*, 78, 16401.
- Gurevich, A. V., L. P. Pitaevskii, and V. V. Smirnova (1969), Ionospheric aerodynamics, *Space Sci. Rev.*, 9(6), 805–871.
- Hasegawa, A. (1975), *Plasma Instabilities and Nonlinear Effects*, Springer-Verlag, Berlin Heidelberg.
- Hastings, D. E. (1995), A review of plasma interactions with spacecraft in low Earth orbit, *J. Geophys. Res.*, 100(A8), 14457–14483.
- Hey, J. S., S. J. Parsons, and J. W. Phillips (1946), Fluctuations in cosmic radiation at radio-frequencies, *Nature*, 158(4007), 234–234, doi:10.1038/158234a0.
- Hockney, R. W., and J. W. Eastwood (1988), *Computer Simulation Using Particles*, CRC Press, IOP Publ., New York.
- Hoegy, W. R., and L. E. Wharton (1973), Current to a moving cylindrical electrostatic probe, *J. Appl. Phys.*, 44(12), 5365–5371.
- Holmström, M., S. Fatemi, Y. Futaana, and H. Nilsson (2012), The interaction between the moon and the solar wind, *Earth Planets Space*, 64(2), 17.
- Ishihara, O., and S. V. Vladimirov (1997), Wake potential of a dust grain in a plasma with ion flow, *Phys. Plasmas*, 4(1), 69–74.
- Jardin, S. (2010), *Computational Methods in Plasma Physics*, CRC Press, Boca Raton, Fla.
- Kintner, P. M., B. M. Ledvina, and E. R. de Paula (2007), GPS and ionospheric scintillations, *Space Weather*, 5, S09003, doi:10.1029/2006SW000260.
- Lafon, J. P. (1973), On the perturbation of a plasma and particle collection by a cylinder in a magnetic field, *J. Plasma Physics*, 10(3), 383–396.
- Laframboise, J. G., and J. Rubinstein (1976), Theory of a cylindrical probe in a collisionless magnetoplasma, *Phys. Fluids*, 19(12), 1900–1908.
- Lehnert, B. (1956), Electrodynamical effects connected with the motion of a satellite of the earth, *Tellus*, 3, 408–409.
- Lemons, D. S., M. S. Murillo, W. Daughton, and D. Winske (2000), Two-dimensional wake potentials in sub- and supersonic dusty plasmas, *Phys. Plasmas*, 7(6), 2306–2313.
- Lieberman, M. A., and A. J. Lichtenberg (2005), Direct current (DC) sheaths, in *Principles of Plasma Discharges and Materials Processing*, 171 pp., John Wiley, Hoboken, N. J.
- Liu, V. C. (1969), Ionospheric gas dynamics of satellites and diagnostic probes, *Space Sci. Rev.*, 9(4), 423–490.

- Lorentzen, D. A., J. Moen, K. Oksavik, F. Sigernes, Y. Saito, and M. G. Johnsen (2010), In situ measurement of a newly created polar cap patch, *J. Geophys. Res.*, 115, 2156–2202, doi:10.1029/2010JA015710.
- Ludwig, P., W. J. Miloch, H. Kähler, and M. Bonitz (2012), On the wake structure in streaming complex plasmas, *New J. Phys.*, 14(5), 53016.
- Maiorov, S. A., S. V. Vladimirov, and N. F. Cramer (2000), Plasma kinetics around a dust grain in an ion flow, *Phys. Rev. E*, 63(1), 17401.
- Marchand, R. (2012), PTetra, a tool to simulate low orbit satellite-plasma interaction, *IEEE Trans. Plasma Sci.*, 40(2), 217–229.
- Melandø, F., and J. Goree (1995), Polarized supersonic plasma flow simulation for charged bodies such as dust particles and spacecraft, *Phys. Rev.*, 52(5), 5312–5326.
- Meyer-Vernet, N. (1976), Rocket spin effects on the current collected by a cylindrical probe in the ionosphere, *J. Geophys. Res.*, 81(4), 450–456.
- Miller, N. J. (1971), Some implications of satellite spin effects in cylindrical probe measurements, *J. Geophys. Res.*, 77(16), 2851–2861.
- Miloch, W. J. (2010), Wake effects and Mach cones behind objects, *Plasma Phys. Controlled Fusion*, 52(12), 124004.
- Miloch, W. J. (2014), Numerical simulations of dust charging and wakefield effects, *J. Plasma Phys.*, 80(6), 795–801.
- Miloch, W. J., H. L. Pécseli, and J. Trulsen (2007), Numerical simulations of the charging of dust particles by contact with hot plasmas, *Nonlinear Processes Geophys.*, 14(5), 575–586.
- Miloch, W. J., J. Trulsen, and H. L. Pécseli (2008), Numerical studies of ion focusing behind macroscopic obstacles in a supersonic plasma flow, *Phys. Rev. E*, 77(5), 56408.
- Miloch, W. J., N. Gulbrandsen, L. N. Mishra, and Å. Fredriksen (2011), Ion velocity distribution in the sheath and presheath of a biased object in plasma, *Phys. Plasmas*, 18(8), 83502.
- Miyake, Y., and H. Usui (2009), New electromagnetic particle simulation code for the analysis of spacecraft-plasma interactions, *Phys. Plasmas*, 16(6), 62904.
- Miyake, Y., C. M. Cully, H. Usui, and H. Nakashima (2013), Plasma particle simulations of wake formation behind a spacecraft with thin wire booms, *J. Geophys. Res. Space Physics*, 118, 5681–5694, doi:10.1002/jgra.50543.
- Moen, J., K. Oksavik, T. Abe, M. Lester, Y. Saito, T. A. Bekkeng, and K. S. Jacobsen (2012), First in-situ measurements of HF radar echoing targets, *Geophys. Res. Lett.*, 39, L07104, doi:10.1029/2012GL051407.
- Mott-Smith, H. M., and I. Langmuir (1926), The theory of collectors in gaseous discharges, *Phys. Rev.*, 28(4), 727–763.
- Murphy, G. B., S. D. Shawhan, L. A. Frank, N. D'Angelo, D. A. Gurnett, J. M. Grebowsky, D. L. Reasoner, and N. Stone (1983), Interaction of the space shuttle orbiter with the ionospheric plasma, in *Proceedings of the 17th ESLAM Symposium on Spacecraft/Plasma Interactions and Their Influence on Field and Particle Measurements*, vol. 198, pp. 73–78, European Space Agency, Noordwijk, Netherlands.
- Okada, M., Y. Omura, and H. Matsumoto (1995), Computer experiments of spacecraft-plasma interactions in a dilute and high- β_e plasma with a fast plasma flow, *J. Geophys. Res.*, 100(A11), 21549–21559.
- Oksavik, K., J. Moen, M. Lester, T. A. Bekkeng, and J. K. Bekkeng (2012), In situ measurements of plasma irregularity growth in the cusp ionosphere, *J. Geophys. Res.*, 117, A11301, doi:10.1029/2012JA017835.
- Olsen, R. C., C. R. Chappell, and J. L. Burch (1986), Aperture plane potential control for thermal ion measurements, *J. Geophys. Res.*, 91(A3), 3117–3129.
- Oya, H. (1970), Ionospheric plasma disturbances due to a moving space vehicle, *Planet. Space Sci.*, 18(6), 793–802.
- Parker, L. W., and B. L. Murphy (1967), Potential buildup on an electron-emitting ionospheric satellite, *J. Geophys. Res.*, 72(5), 1631–1636.
- Patacchini, L., and I. H. Hutchinson (2011), Spherical conducting probes in finite Debye length plasmas and $E \times B$ fields, *Plasma Phys. Controlled Fusion*, 53(2), 025005.
- Pécseli H. L. (2013), *Waves and Oscillations in Plasmas*, CRC Press, Hoboken, N. J.
- Prikryl, P., P. T. Jayachandran, S. C. Mushini, and R. Chadwick (2011), Climatology of GPS phase scintillation and HF radar backscatter for the high-latitude ionosphere under solar minimum conditions, *Ann. Geophys.*, 29(2), 377–392, doi:10.5194/angeo-29-377-2011.
- Riemann, K. U. (1991), The Bohm criterion and sheath formation, *J. Phys. D: Appl. Phys.*, 24, 492–518.
- Rubinstein, J., and J. G. Laframboise (1983), Theory of axially symmetric probes in a collisionless magnetoplasma: Aligned spheroids, finite cylinders, and disks, *Phys. Fluids*, 26(12), 3624–3627.
- Samir, U., and G. L. Wrenn (1972), Experimental evidence of an electron temperature enhancement in the wake of an ionospheric satellite, *Planet. Space Sci.*, 20(6), 899–904.
- Sanmartin, J. R. (1970), Theory of a probe in a strong magnetic field, *Phys. Fluids*, 13(1), 103–116.
- Siskind, D. E., W. J. Raitt, P. M. Banks, and P. R. Williamson (1984), Interactions between the orbiting space shuttle and the ionosphere, *Planet. Space Sci.*, 32(7), 881–896.
- Spicher, A., W. J. Miloch, L. B. N. Clausen, and J. I. Moen (2015), Plasma turbulence and coherent structures in the polar cap observed by the ICI-2 sounding rocket, *J. Geophys. Res. Space Physics*, 120, 10,959–10,978, doi:10.1002/2015JA021634.
- Spicher, A., A. A. Ilyasov, W. J. Miloch, A. A. Chernyshov, L. B. N. Clausen, J. I. Moen, T. Abe, and Y. Saito (2016), Reverse flow events and small-scale effects in the cusp ionosphere, *J. Geophys. Res. Space Physics*, 121, 10,466–10,480, doi:10.1002/2016JA022999.
- Stone, N. H., (1981), The aerodynamics of bodies in a rarefied ionized gas with applications to spacecraft environmental dynamics, Tech. Rep. TP-1933, NASA Marshall Space Flight Center, Huntsville, Ala.
- Sugawara, M. (1998), *Plasma Etching: Fundamentals and Applications*, Oxford Univ. Press, New York.
- Svenes, K. R., J. Trim, B. N. Maehlum, M. Friedrich, K. M. Torkar, G. Holmgren, and W. F. Denig (1990), Ram-wake measurements obtained from the ionospheric sounding rocket MAIMIK, *Planet. Space Sci.*, 38(5), 653–663.
- Svenes, K. R., and J. Troim (1994), Laboratory simulation of vehicle-plasma interaction in low Earth orbit, *Planet. Space Sci.*, 42(1), 81–94.
- Szuszczewicz, E. P., and P. Z. Takacs (1979), Magnetosheath effects on cylindrical Langmuir probes, *Phys. Fluids*, 22(12), 2424–2429.
- Tajima, T. (1989), *Computational Plasma Physics: With Applications to Fusion and Astrophysics*, Frontiers in Physics, vol. 72, Addison-Wesley, Redwood City, Calif.
- Tang, X-Z., and G. L. Delzanno (2014), Orbital-motion-limited theory of dust charging and plasma response, *Phys. Plasmas*, 21(12), 123708.
- Temerin, M., and P. M. Kintner (1989), Review of ionospheric turbulence, in *Plasma Waves and Instabilities at Comets in Magnetospheres*, pp. 65–80, Wiley Online Library, Washington, D. C.
- Vladimirov, S. V., and M. Nambu (1995), Attraction of charged particulates in plasmas with finite flows, *Phys. Rev. E*, 52(3), R2172–R2174.
- Wang, J., and D. E. Hastings (1992), Ionospheric plasma flow over large high voltage space platforms. II: The formation and structure of plasma wake, *Phys. Fluids B*, 4(6), 1615–1629.

- Whipple, E. C. (1965), The equilibrium electric potential of a body in the upper atmosphere and in interplanetary space, PhD thesis, George Washington Univ., Washington, D. C.
- Whipple, E. C. (1981), Potentials of surfaces in space, *Rep. Prog. Phys.*, 44(11), 1197–1250.
- Yamamoto, M. Y. (2001), Study on the wake structure and associated plasma wave turbulence observed by using sounding rocket experiments, PhD thesis, Tohoku Univ., Sendai, Japan.
- Yaroshenko, V. V., W. J. Miloch, H. M. Thomas, and G. E. Morfill (2012), Cassini capturing of freshly-produced water-group ions in the Enceladus torus, *Geophys. Res. Lett.*, 39, L18108, doi:10.1029/2012GL053173.